Journal of Power Sources 196 (2011) 7144–7151

Contents lists available at ScienceDirect

Journal of Power Sources

journal homepage: www.elsevier.com/locate/jpowsour

Impact of naphthalene on the performance of SOFCs during operation with synthetic wood gas

Martin Hauth*, Werner Lerch, Karlheinz König, Jürgen Karl

Graz University of Technology, Institute of Thermal Engineering, Inffeldgasse 25/B, 8010 Graz, Austria

ARTICLE INFO

Article history:
Received 8 June 2010
Received in revised form 1 September 2010
Accepted 2 September 2010
Available online 15 September 2010

Keywords:
SOFC
Tar
Reforming
Hydrocarbon
Naphthalene
Fuel utilization

ABSTRACT

The ability of solid oxide fuel cells to convert not only H_2 but also CO and its utilization of a catalyst containing anode enabling the conversion of hydrocarbon fuels allows the use of wood gas. The hydrocarbons in the wood gas show the ability to be converted to H_2 and CO directly to a certain extent due to reforming reactions. Therefore the available amount of H_2 and CO at the anode is depending to what degree the hydrocarbons become reformed. In order to illustrate the impact of a varying hydrocarbon content and consequently of a varying available amount of H_2 and CO on the fuel utilization due to individual reforming rates, the performed tests with synthetic wood gas and varying naphthalene contents using a single-cell test rig are presented. The conversion of naphthalene impacts not only the open circuit voltage but also the cell voltage during operation. Therefore this paper focuses on the change of the cell voltage due to a changing available amount of H_2 and CO resulting from reforming of naphthalene and methane. The experimental results are compared with theoretical equilibrium calculations to illustrate the kinetic impact of the process parameters on the reforming mechanism.

1. Introduction

Great effort has been undertaken in the past to understand the mechanisms to use hydrocarbon fuels in solid oxide fuel cells (SOFCs) [1–15]. This is an important step for the commercialization of SOFCs using any kind of hydrocarbon fuels based on fossil fuels such as natural gas, jet fuel, coal gas or on biomass fuels such as wood gas from biomass gasification, biogas from fermentation or methanol.

A promising way to produce electricity from biomass is the coupling of a biomass gasifier linked with a SOFC system [16]. Allothermal steam gasification provides a hydrogen rich wood gas with a high water content [17,18] turning the wood gas into an attractive fuel opportunity for SOFC systems. Due to the impurities in the wood gas (sulfur, alkali, chlorine, particles, tars) a gas cleaning unit to some extent is necessary [19]. Exact operation limits for all impurities regarding the anode of a SOFC system are not entirely determined yet. However, experiments with different wood gas compositions of various types of gasifiers show a surprisingly high tolerance of the SOFC anode towards higher hydrocarbons, so called tars, even containing aromatic compounds [20–22]. The possibility of tar conversion in a SOFC not only significantly simplifies the gas cleaning unit but also enables the direct use of the produced heat for the endothermic steam reforming reaction at the anode surface and thus increases the overall efficiency of the system.

Most investigations regarding the use of hydrocarbons in SOFCs through steam reforming are either heterogeneous catalysis experiments or tests on SOFC anodes at open circuit voltage, whereas the effect of the drawn current on the steam reforming reaction is not intensively investigated yet. Furthermore, the reforming kinetics depending on the structure of the hydrocarbon are very complex. Frank [1] for example shows that the addition of naphthalene inhibits the conversion of methane and toluene on a SOFC anode. So far there are only few studies about the mutual interference of the hydrocarbons in the steam reforming reaction on a SOFC anode.

These two topics - inhibited reforming rates due to certain combinations of hydrocarbons in the fuel mixture and the impact of the current density on the reforming mechanism – need to be investigated in order to quantify the influence on the fuel utilization during high loads due to inhibited reforming kinetics with respect to the nickel oxidation boundary. In order to be able to predict the possible maximum fuel utilization rate to securely avoid nickel oxidation the amount of additional H_2 and CO coming from the reforming reactions has to be known. Assuming the SOFC operating at a constant current density the fuel utilization depends very much on the reforming rate.

This work focuses on the conversion of naphthalene as a model tar in tests with synthetic wood gas. Naphthalene accounts for a large amount of the entire tar content in the wood gas. Therefore, the conversion rate for various concentrations of naphthalene

* Corresponding author.
E-mail address: martin.hauth@tugraz.at (M. Hauth).

0378-7753/$ – see front matter © 2010 Elsevier B.V. All rights reserved.
doi:10.1016/j.jpowsour.2010.09.007

mixed into a $H_2/H_2O/N_2$ fuel gas is shown in a single cell test rig for planar $10 \times 10\,cm^2$ Ni-GDC/YSZ/LSM[1] cells for 800 and 900 °C. Further tests with a mixture of synthetic wood gas show the impact of naphthalene on methane reforming. This particular effect of the reforming behaviour to the fuel utilization considering nickel oxidation is applied to a ternary plot for the constituents H–C–O.

2. Scientific approach

The investigation of the impact of naphthalene on steam reforming when operating a SOFC with synthetic wood gas necessitates a clear understanding of what is meant in this work by the conversion rate and reforming rate respectively of naphthalene and methane. This conversion rate gives information about the converted amount of hydrocarbon present in the fuel gas that is eventually increasing the electrochemical potential.

Here, FID[2] measurements, gas analysis and cell voltage measurements are taken to illustrate the conversion of hydrocarbons. A combination of these methods allows a better suggestion to what extent the reforming reaction only occurs while considering other reactions such as the shift reaction or carbon deposition. In order to quantify the impact of the nickel meshes used for current collection at the anode side on the reforming mechanism, tests without nickel meshes have been performed. The results show the ability of the anode layer alone to reform hydrocarbons.

The conversion rate is an important parameter when operating the SOFC under high fuel utilization rates. Particularly the fuel utilization can change significantly depending on to what degree the hydrocarbons become reformed. In order to quantify the change of the fuel utilization due to varying reforming rates caused by varying amounts and types of hydrocarbons it is necessary to compare performance results from hydrocarbon free fuel gas with hydrocarbon loaded fuel gas.

Operating the SOFC at high fuel utilization rates implicates the risk of nickel oxidation. To show the influence of the conversion rate to the fuel utilization and further illustrate the critical distance of the operation point to the nickel oxidation boundary the results from the measurements are taken to build a theoretical scenario based on equilibrium calculations.

2.1. Conversion rate of naphthalene and methane

In the atmosphere inside the anode chamber that is perfused by a gas mixture of $H_2/H_2O/N_2$ and small amounts of $C_{10}H_8$ various reaction pathways for the hydrocarbon are possible. Depending on the H_2O content mainly carbon deposition, reforming and the shift reaction are favorable on a nickel catalyst. For high H_2O contents (as in the experiments described here) where carbon deposition is thermodynamically not predicted a sequence of the reforming reaction followed by the shift reaction is assumed. In order to define the reforming rate one would have to look at the conversion of the hydrocarbon to H_2 and CO only. The following shift reaction does not allow an isolated observation of the reforming rate using H_2 and CO gas analysis at the anode outlet. The appearance of CO_2 in the anode outlet at open circuit conditions for example suggests further conversion of CO using H_2O after the reforming step.

Therefore the concentration of naphthalene at the anode outlet is measured and compared with the anode inlet. Assuming carbon deposition does not occur, the consumption of naphthalene correlates to the amount that is being reformed. Because of the change of H_2 and H_2O along the reaction affecting the FID signal due to cross-sensitivity effects, the outlet concentration of H_2O need to be measured as well in order to calculate the real C_xH_y load at the anode outlet. However, the failure is minor and thus H_2O measurements at the outlet are not carried out. Hence, in this work a conversion rate rather than a reforming rate based on the FID signal is defined as,

$$CR = \frac{(\nu_{CxHy,inlet} - \nu_{CxHy,outlet})}{\nu_{CxHy,inlet}} \quad (1)$$

where CR is in % and ν_{CxHy} is in ppm. All values in this paper given in ppm are based on the volumetric part. In this case CR for methane and naphthalene is intended to be calculated.

2.2. H_2-utilization with $H_2/N_2/H_2O/C_{10}H_8$ at 900 °C

The impact of the current density to steam reforming is shown by V-i curves for a mixture of 23.3% H_2, 19.5% H_2O, balance N_2 and a naphthalene content of 3606 ppm at 900 °C. This experiment gives information whether or not the oxygen ion flow at increased current densities interacts with the reforming reaction. Further, the impact of varying conversion rates on the H_2-utilization is investigated in order to illustrate the hazard of nickel oxidation during constant current operation conditions. Wood gas from biomass gasification usually shows varying tar contents resulting from the discontinuous gasification process [23]. Using wood gas would mean a continuously alternating amount of H_2 and CO available at the anode leading to critical H_2-utilization rates. The H_2-utilization rate is defined as,

$$U_{fH2} = \frac{(\nu_{H2,inlet} - \nu_{H2,outlet})}{\nu_{H2,inlet}} \quad (2)$$

where $U_{f,H2}$ is in % and ν_{H2} in %(vol).

2.3. H_2-utilization with synthetic wood gas at 900 °C

A gas mixture of 20.8% H_2, 13.3% CO, 13.3% CO_2, 6.3% CH_4, 26.8% H_2O, balance N_2 and 2032 ppm $C_{10}H_8$ as a model tar represents the tested synthetic wood gas. Numerous tests so far concentrated on the conversion of methane in a $H_2/N_2/H_2O$ feed. However, CO and CO_2 play an important role due to the possibility of dry reforming and the shift reaction. Moreover, increased levels of CO involve the risk of the Boudouard reaction which results in carbon formation.

In this particular case the competitive reforming reaction of naphthalene and methane is focused at. An inhibition of methane reforming due to the presence of naphthalene is shown by various process parameters such as cell temperature, cell voltage and outlet concentration of the hydrocarbon mix. Similar to the $H_2/H_2O/N_2/C_{10}H_8$ gas mix described before V-i curves in combination with curves for the H_2-utilization are brought.

2.4. Theoretical scenario regarding nickel oxidation due to naphthalene reforming

The results of the investigations considering the change of the H_2-utilization depending on the gas mix are joined and used to point out a possible scenario regarding the hazard of nickel oxidation for synthetic wood gas operation. Lines for the equilibrium concentrations under electrical load are drawn into a ternary H–C–O plot to enable an illustration of the critical distance d_{NiO} that is left before nickel oxidation is thermodynamically predicted.

Such a plot can be supportive in order to define critical tar loads as well as initiate control strategies focused on the avoidance of critical H_2-utilization rates.

[1] GDC: gadolinium doped ceria, YSZ: yttria stabilized zirconia, LSM: lanthanum strontium manganite.

[2] FID: Flame Ionic Detector.

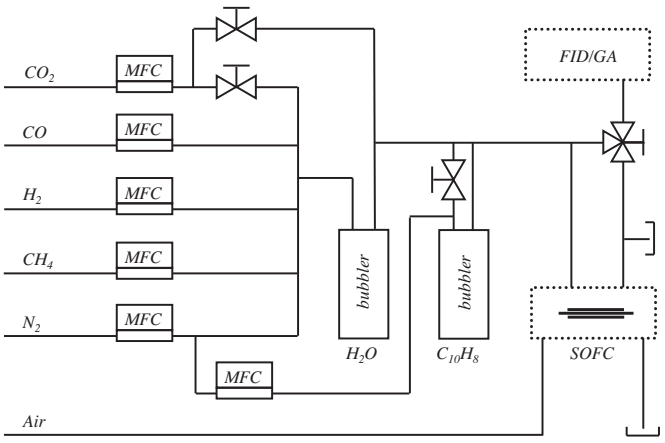

Fig. 1. Scheme of the SOFC test rig.
MFC: Mass Flow Controller; FID: Flame Ionization Detector; GA: Gas Analyzer.

3. Experimental setup

The experiments are supposed to simulate the behaviour of wood gas from biomass gasification on a SOFC anode. Therefore synthetic wood gas consisting H_2, CO, CH_4, CO_2 and N_2 are mixed using five mass flow controllers. The scheme of the test rig is shown in Fig. 1. The gas mixture becomes humidified by a water bubbler which is temperature controlled and monitored by a humidity sensor on the outlet of the humidifier. Due to the capability of CO_2 adsorption of water CO_2 is by-passed at the humidifier. For operation with naphthalene an additional N_2 stream flows through a temperature controlled naphthalene bubbler. The concentration of naphthalene is varied by changing the N_2 flow through the naphthalene bubbler. N_2 for the naphthalene bubbler is branched after the mass flow controller of the main N_2 inlet in order to achieve constant N_2 concentrations in the final gas mixture while varying the N_2 flow through the naphthalene bubbler. The N_2 flow through the naphthalene bubbler is controlled with a mass flow controller. The saturated $N_2/C_{10}H_8$ mixture is then conflated with the humidified synthetic wood gas. To enable a constant humidifier temperature and thus a better comparability the N_2 flow through the naphthalene bubbler is by-passed during tests without naphthalene.

The naphthalene loaded synthetic wood gas then is directed through stainless steel pipes at 150 °C to an oven containing the ceramic cell housing. Before the gas enters the anode chamber it is heated up in a ceramic tube and reaches operation temperature. For the cathode supply dry synthetic air ($20\%O_2/80\%N_2$) is provided. The single cell housing consists of Al_2O_3 and carries a commercial planar $10 \times 10\,cm^2$ Ni-GDC/YSZ/LSM electrolyte supported cell. The porous NiO/GDC anode layer is 30–50 μm thick. The electrolyte layer consists of 8 mol% Y_2O_3 doped ZrO_2 and has a thickness of 80–110 μm. On the cathode side two porous layers are used. The layer touching the electrolyte consists of 8 mol% Y_2O_3 doped ZrO_2 mixed with LSM followed by a pure LSM layer. Gas sealing is achieved using planar surfaces between the electrolyte and the ceramic housing. A weight of approximately 15 kg is applied on top of the ceramic housing.

Current collection is attained by laying the coarse nickel mesh, the fine nickel mesh, the nickel foam and the anode side of the cell on top of each other. In the same way the coarse platinum mesh, the fine platinum mesh, the cathode paste and the cathode side of the cell is positioned. The nickel mesh on the anode side as well as the platinum mesh on the cathode side is connected via platinum wires to the electrical load. Two further platinum wires are used for voltage measurements. At the anode side the feed-through of the platinum wires through the ceramic housing are closed with ceramic paste.

The gas concentration before and after the anode chamber is alternately measured either by a FID (Bernath Atomic 3005) to determine the concentration of the hydrocarbons or by a GA (ABB Advance Optima 2000) to obtain the concentration of the permanent gases. The FID measures the propane gas equivalence which is later meant by "raw" FID signal. To obtain the exact C_xH_y concentration the signal needs to be converted considering the type of hydrocarbon measured and the cross-sensitivity effects of H_2 and H_2O.

4. Results and discussion

4.1. Open circuit voltage with $H_2/N_2/H_2O/C_{10}H_8$ at 800 and 900 °C

Fig. 2 shows the voltage increase for a gas mixture of 23.3% H_2, 19.5% H_2O, balance N_2 and a varying $C_{10}H_8$ concentration at 800 and 900 °C. In this diagram the voltage increase stands for the difference of the open circuit voltage between operation with and without naphthalene while keeping the H_2 and H_2O concentration constant. In these four test series the $C_{10}H_8$ inlet concentration amounts to 483, 1113, 2118 and 3606 ppm respectively. Further the calculated Nernst voltage increase expected from equilibrium calculations for open circuit conditions is given for comparison.

Naphthalene is expected to become partly reformed on the nickel catalyst surface of the anode using H_2O. Therefore H_2 and CO is produced due to the reforming reaction. The shift reaction converts part of the CO to CO_2 and H_2 using H_2O. This increase of H_2 and CO means further fuel for the fuel cell which consequently leads to an increased open circuit voltage as predicted by equilibrium calculations [24].

A clear dependency of the naphthalene reforming activity on the cell temperature becomes obvious when comparing the two curves for 800 and 900 °C in Fig. 2. More naphthalene is converted at 900 °C then at 800 °C. Therefore the increase of the open circuit voltage is smaller at 800 °C. A linear increase of the open circuit voltage with rising naphthalene content is not only predicted by equilibrium calculations as shown in Fig. 2 (dotted lines) but can also be observed from the real measured data (solid lines).

Good comparability provide the results from Frank [1] showing experiments with methane, naphthalene, phenol and toluene over a Ni-GDC anode between 650 and 850 °C. The conversion rate

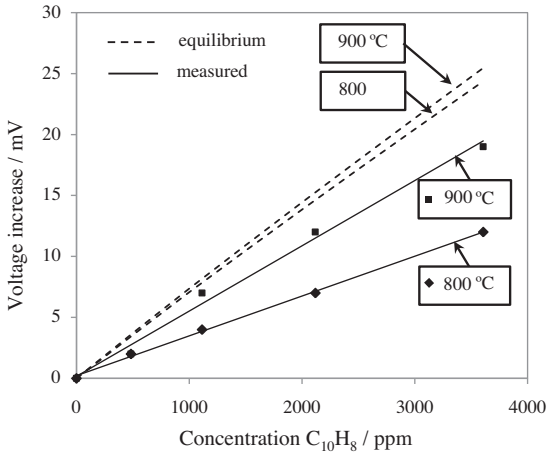

Fig. 2. Increase of the Open Circuit Voltage due to reforming of naphthalene for a gas mixture of 23.3%H_2, 19.5%H_2O, balance N_2 and a varying $C_{10}H_8$ concentration (483, 1113, 2118 and 3606 ppm(vol)) at 800 and 900 °C.

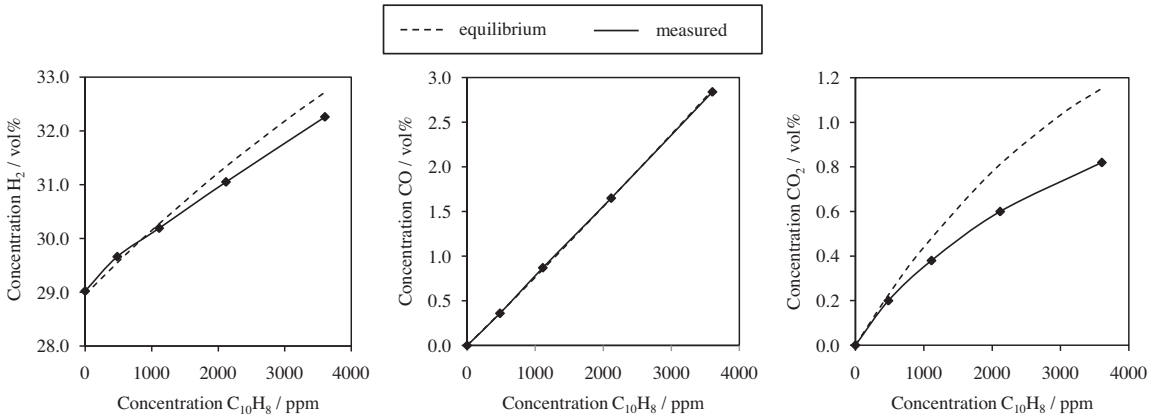

Fig. 3. Comparison of the measured (solid lines) and equilibrium (dotted lines) anode outlet concentration of H_2, CO and CO_2 at open circuit for a fuel gas of 23.3%H_2, 19.5%H_2O, balance N_2 and a varying $C_{10}H_8$ concentration (483, 1113, 2118 and 3606 ppm(vol)) at 900 °C.

is illustrated by measuring the open circuit voltage for separate components and several mixtures. A voltage increase caused by the reforming of hydrocarbons depending on the cell temperature could be detected. This temperature depending conversion rate is also observed in heterogeneous catalysis experiments on nickel catalysts from Jess [25] for naphthalene, benzene and methane. Compared to pyrolysis results the conversion temperature for naphthalene is significantly lower and is located between ~600 and 800 °C by experiments of Jess [25,26].

This behaviour is underlined when looking at the gas concentrations at the anode outlet. The naphthalene concentration after the anode is lower for 900 °C compared to 800 °C. Nevertheless, the conversion rate indicates that relatively less naphthalene becomes reformed the higher the inlet concentration of naphthalene is. The conversion rate at 900 °C using the raw FID signal is ~100, 99.7, 98.7 and 97.3% for 483, 1113, 2118 and 3606 ppm respectively. Hence one could expect that the open circuit voltage increased other than linearly for even higher naphthalene concentrations. Analyzing the H_2, CO and CO_2 concentration after the anode and comparing it to the equilibrium concentration corresponds to the idea of a temperature depending conversion rate. H_2 and CO_2 being below equilibrium concentration (s. Fig. 3) differs more the higher the naphthalene concentration is showing a similar non-linear characteristic as seen from the FID signal. The gaps between the measured values and equilibrium are smaller at 900 °C than at 800 °C. CO nearly matches equilibrium concentration which could occur due to a limited reforming reaction combined with a limited shift reaction. In this case less CO is produced by reforming followed by a lower consumption due to the shift reaction.

4.2. H_2-utilization with $H_2/N_2/H_2O/C_{10}H_8$ at 900 °C

When measuring the cell voltage in operation a constantly higher cell voltage due to the reforming of naphthalene compared to operation without naphthalene can be observed over a current density range of 0 to 190 mA/cm^2 (s. Fig. 4, left). In operation oxygen ions migrate from the cathode to the anode side and interact with the adsorbed fuel components such as H and CO on the catalyst surface [27]. Koh et al. [7] even demonstrated that the oxygen ions react with deposited carbon and thus cell degradation will be reduced. Since the steam reforming mechanism occurs on the catalyst surface according to Xu et al. [28] it needs to be tested whether a likewise reaction between the oxygen ions and the adsorbed hydrocarbons in case of slow reaction kinetic as it is assumed in the case of naphthalene is possible. Similar to the reaction scenario from Koh et al. [7] for deposited carbon that assumes the possibility of carbon oxidation only near the triple phase boundary due to the reduced oxygen conduction of nickel, the impact of the current density on the conversion of hydrocarbons is likely to be limited. The produced water from the electrochemical reaction of H_2 could support the reforming reaction. Nevertheless, the water contend in the inlet gas stream (19.5%) is theoretically high enough to enable complete reforming and avoid carbon formation.

No impact of the operation with current on the reforming reaction can be derived from the gas analysis and the cell voltage. The observed stepwise changes in the FID outlet signal when increasing the current density are small and might be due to the change of H_2 and H_2O content in the anode off gas (both H_2 and H_2O have cross-sensitivity effects on the FID signal).

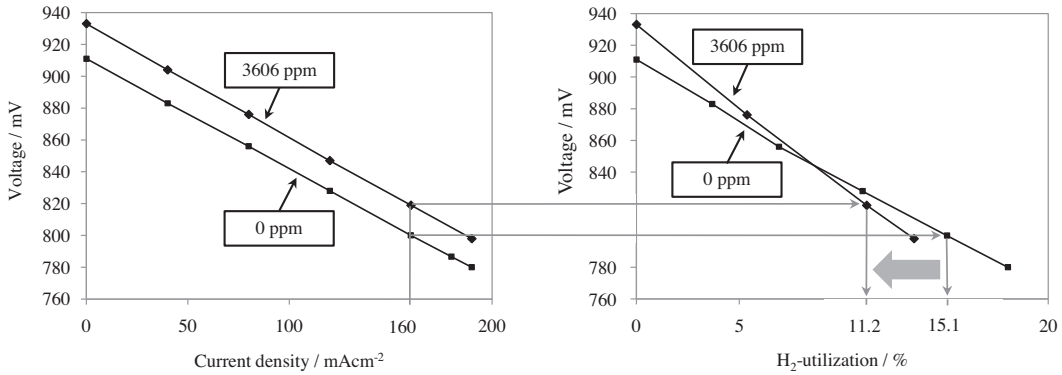

Fig. 4. Impact of naphthalene reforming on the cell voltage (left) and the H_2-utilization rate (right) for a gas mixture of 23.3%H_2, 19.5%H_2O, balance N_2 and 0/3606 ppm(vol) $C_{10}H_8$ at 900 °C at a constant gas flow.

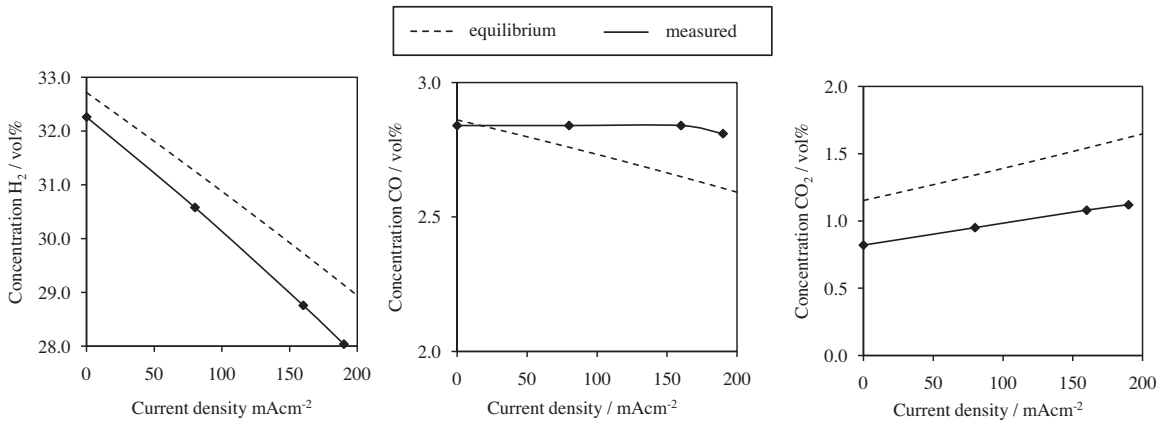

Fig. 5. Comparison of the measured (solid lines) and equilibrium (dotted lines) anode outlet concentration of H_2, CO and CO_2 at operation for a fuel gas of 23.3%H_2, 19.5%H_2O, balance N_2 and 3606 ppm(vol) $C_{10}H_8$ at 900 °C.

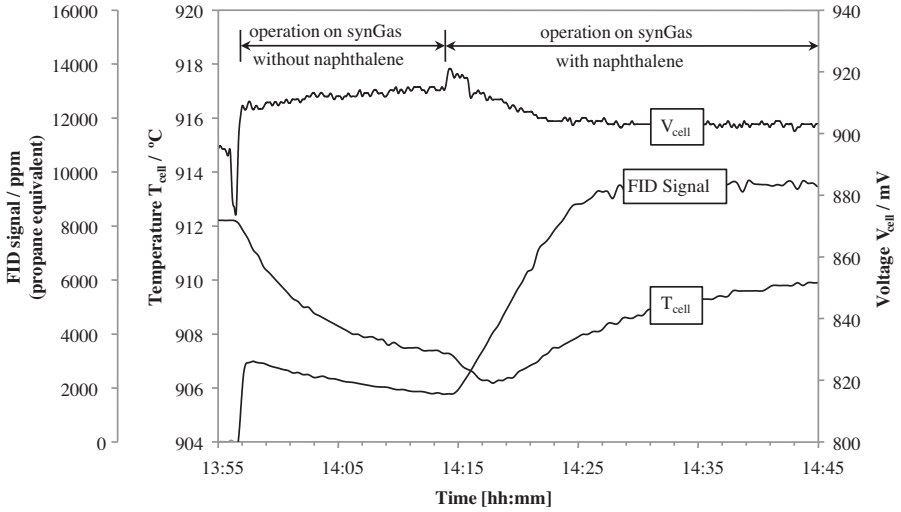

Fig. 6. Impact of 2032 ppm(vol) naphthalene on the conversion rate of methane in synthetic wood gas (20.8%H_2, 13.3%CO, 13.3%CO_2, 6.3%CH_4, 26.8%H_2O, balance N_2) at 900 °C.

Fig. 4 (right) explains the impact of the reforming reaction on the H_2-utilization. As stated by Laosiripojana [6] the produced H_2 and CO from reforming become electrochemically consumed. However, here, CO is not considered because CO consumption is hardly observed from the analysis of the anode exhaust composition with increasing current density at 900 °C as shown in Fig. 5. The CO concentration at the anode outlet stays almost constant while H_2 gets steadily consumed. CO_2 on the other hand increases with increasing current density indicating either electrochemical oxidation of CO or an enhanced shift reaction. However, both cases would require the consumption of CO. Another possibility would be the oxidation of deposited carbon or adsorbed naphthalene. Nevertheless, since carbon deposition was not the main focus of this work no further investigations such as SEM[3] micrographs are carried out.

Running the SOFC under a constant load of 160 mA/cm^2 a H_2-utilization rate of 15.1% is reached when operating with a naphthalene free gas (s. Fig. 4). For an identical current density, the same gas composition with 3606 ppm naphthalene achieves a H_2-utilization rate of 11.2%. This can be attributed to additional H_2 coming from naphthalene reforming. In terms of nickel oxidation this can be an important factor when operating the SOFC at high H_2-utilization rates. A sudden increase of the H_2-utilization rate due to a varying tar content during constant current operation with real wood gas could destroy the anode irreversibly.

4.3. H_2-utilization with synthetic wood gas at 900 °C

A synthetic wood gas containing 20.8%H_2, 13.3%CO, 13.3%CO_2, 6.3%CH_4, 26.8%H_2O and balance N_2 is used to represent wood gas from biomass gasification. The feed contains either 0 or 2032 ppm naphthalene. Fig. 6 shows the curves for the cell voltage, cell temperature and the raw FID signal (propane gas equivalence). Initially (13:55–14:15, time of day) the cell is constantly supplied with the naphthalene free synthetic wood gas. Approximately one minute after starting to apply the synthetic wood gas a sudden decrease of the cell temperature is monitored. This is caused by the endothermic reforming reaction of methane. Furthermore the FID signal representing the anode outlet concentration of methane rises immediately and is quickly followed by a steady decrease. It seems that more methane becomes converted as time progresses. The gas analyzer (GA) confirms this effect. It takes approximately 2 hours until steady state is reached. A similar trend for methane is reported from Finnerty and Ormerod [9]. This behaviour is inverse to the reforming of naphthalene where the FID signal would first rise and then slowly approach a maximum value within an hour depending on the naphthalene concentration. A significant increase after switching to synthetic wood gas can be observed as well for

[3] SEM: Scanning Electron Microscope.

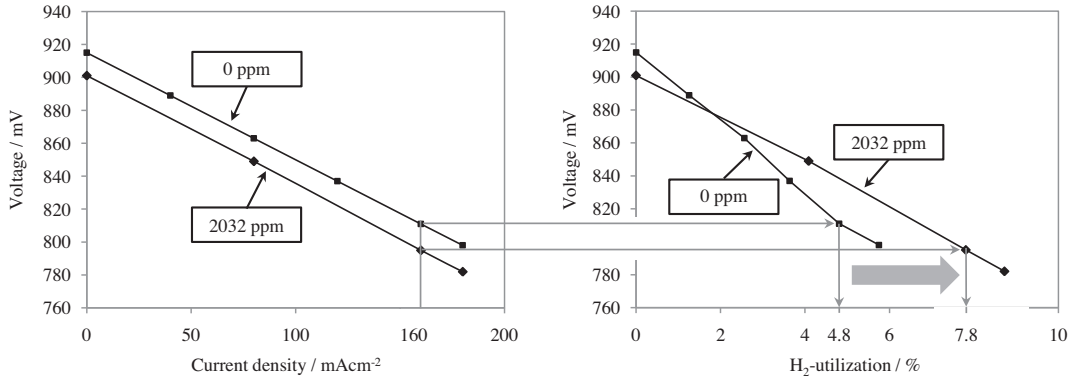

Fig. 7. Impact of naphthalene reforming on the cell voltage (left) and the H_2-utilization rate (right) for synthetic wood gas (20.8%H_2, 13.3%CO, 13.3%CO_2, 6.3%CH_4, 26.8%H_2O, balance N_2 and 0/2032 ppm(vol) $C_{10}H_8$) at 900 °C at a constant gas flow.

the cell voltage indicating a higher H_2 and CO content due to steam reforming of methane. The cell voltage rises steadily in the same way as the CH_4 outlet concentration decreases, which is again different to naphthalene where the cell voltage stays constant while the naphthalene outlet concentration rises in the beginning.

After 20 min (14:15–14:45) 2032 ppm naphthalene are added to the synthetic wood gas leaving the rest constant. The immediately increasing cell temperature and FID signal as well as the drop of the cell voltage suggests an inhibition of the methane reforming mechanism due to the competing reforming reaction of naphthalene. Frank [1] for example shows that combinations of naphthalene, toluene and methane in a biogenous gas mixture resulted in an inhibited conversion of methane and toluene in the presence of naphthalene. Jess and Deppner [25,29] illustrate the competitive reaction between naphthalene and methane being naphthalene the most reactive. In their case methane becomes reformed not until the temperature where complete naphthalene conversion is reached. Similar behaviour can be found for dodecane and tetralin by Gould et al. [11]. The substances were tested individually and in a 50/50% mixture in a quartz tube reactor over a $Ni/Ce_{0.75}Zr_{0.25}O_2$ catalyst. The autothermal reforming experiments show that the conversion rate of the mixture is not a linear combination of those of the pure substances but rather close to the behaviour as received from pure tetralin. Shekhawat et al. [14] finds out that the overall yields from the reforming of a fuel mixture are not additive of yields from individual fuel components rather the more reactive component is consumed first.

Since the characteristic of the cell voltage in Fig. 6 accords with that of the FID signal, the reforming products rather than the change of the cell temperature are seen to be the main reason for the increasing and decreasing cell voltage. Measurements of the CH_4 concentration in another similar test show a constant outlet concentration of 5.1% CH_4 while adding naphthalene to the synthetic wood gas. As soon as naphthalene is turned off the CH_4 concentration at the anode outlet steadily decreases over a period of half an hour until approaching a constant value. This behavior is supported by the heterogeneous catalysis model for methane steam reforming suggested from Xu et al. [28]. The steps of the reaction mechanims are: adsorption of methane on the Ni surface, decomposition, surface reaction and desorption of the products from the Ni surface. Xu postulates that kinetic inhibition due to the many steps of the reforming reaction can lead to a decreasing reactive surface caused by the adsorption on the Ni particle.

In the here described experiment the adsorption and desorption of naphthalene is obviously interfering with the reforming of methane by decreasing the reactive surface. An estimation to what extent naphthalene becomes reformed in the presence of methane is difficult since the FID detects the sum of all hydrocarbons. According to the tests described before with 23.3%H_2, 19.5%H_2O, balance N_2 and 2118 ppm at 900 °C almost complete conversion (98.7%) for naphthalene can be expected. Comparing the FID signal with CH_4 gas analysis supports the assumption of complete naphthalene conversion.

Fig. 7 (left) similarly to Fig. 4 (left) shows the impact of naphthalene reforming on the cell voltage when applying an electrical load. The upper curve representing the naphthalene free synthetic wood gas achieves higher voltages compared to the bottom curve where naphthalene is added. In this case the addition of naphthalene leads to a decreased cell voltage due to the before mentioned reason. The behaviour is inverse compared to the one described in Fig. 4. Considering the inhibition of methane reforming, a conversion rate of naphthalene of 98.7% (as achieved from the experiment with 23.3%H_2, 19.5%H_2O, balance N_2 and 2118 ppm at 900 °C) and the slightly different cell temperatures between those two experiments a theoretical Nernst voltage decrease of 11 mV can be calculated compared to 15 mV cell voltage decrease measured at open circuit conditions.

The difference of the cell voltage as well as of the theoretical Nernst voltage stays constant with increasing current density. Therefore it is assumed that the oxygen ion flow and the electrochemical reactions do not influence the competing reforming mechanism between naphthalene and methane in a current density range between 0 and 190 mA/cm^2.

As in Fig. 4 (right) the scenario for the H_2-utilization for synthetic wood gas due to naphthalene reforming is illustrated in Fig. 7 (right). The consumption of CO with increasing current density is small while CO_2 production is clearly visible. Comparing the H_2 concentration at a current density of 160 mA/cm^2 indicates a H_2-utilization rate of 4.8% without and 7.8% with naphthalene respectively. In this case addition of naphthalene would increase the hazard of nickel oxidation due to an increasing H_2-utilization rate for operation at a realistic fuel utilization.

However, the H_2-utilization rates shown in Figs. 4 and 7 are low. A different situation regarding the interaction with the reforming reaction could occur at high H_2-utilizations where the H_2 concentration is already low. A lack of highly active H_2 could cause the oxygen to rather react with adsorbed hydrocarbons from adjacent nickel surfaces close to the triple-phase boundary. Therefore similar tests with higher H_2-utilization rates need to be carried out to confirm this behavior for H_2-utilization rates up to 80%.

4.4. Theoretical Scenario regarding nickel oxidation due to naphthalene reforming

Theoretically nickel oxidation during operation starts as soon as there is no fuel left that can be oxidized at the anode. In other

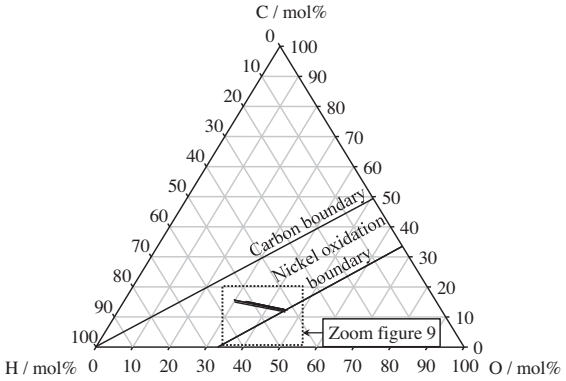

Fig. 8. Ternary H–C–O plot for the equilibrium concentration of three operation curves.

words the oxygen coming from the cathode starts oxidizing the nickel particle due to the lack of H_2 and CO. This can be attributed to a theoretical fuel utilization rate of 100%. In reality such a high fuel utilization rate is not possible due to concentration polarization causing nickel oxidation already at lower fuel utilization rates. A maximum fuel utilization rate of around 80% to avoid nickel oxidation is generally recommended from the literature.

The operation curves can be drawn in a ternary H–C–O plot as shown in Fig. 8 for three different gas compositions based on the scenario constraints described below. For each of the three gas compositions the molecular percentages of H, C and O are calculated for open circuit conditions and operation. When increasing the current density more oxygen comes from the cathode to the anode and the gas composition in the ternary plot moves towards the oxygen corner represented by the operation curves. Along these lines the current density increases linearly. The boundary for carbon deposition as well as for nickel oxidation is indicated in order to illustrate the critical distance towards these two boundaries during operation. The equilibrium boundaries are calculated using FactSage 6.1. The area in the ternary plot above the carbon boundary indicates gas compositions where carbon deposition is thermodynamically predicted whereas in the area below the nickel oxidation boundary the formation of nickel oxides is predicted. According to Figs. 4 and 7 the H_2-utilization rate is used in Fig. 9. For each point on the operation curve the H_2-utilization rate according to the current density is calculated. The H_2-utilization is 0% at 0 mA/cm^2 and rises linearly along the operation curve up to 100% which is the point where the operation curve meets the nickel oxidation boundary.

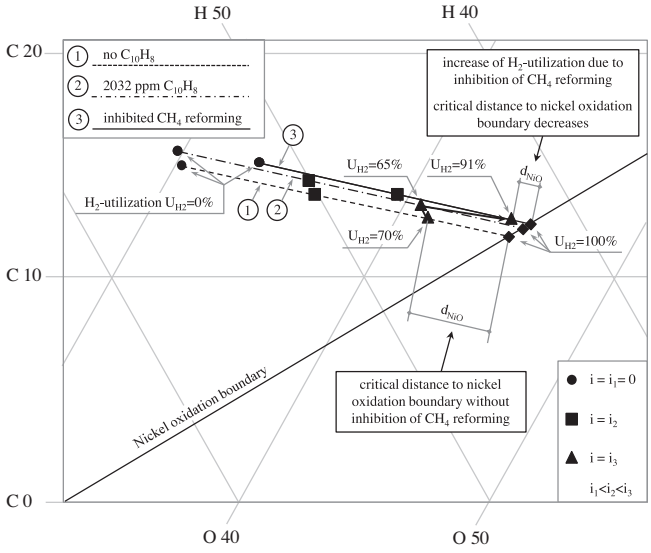

Fig. 9. Theoretical scenario regarding nickel oxidation due to naphthalene reforming for the operation with synthetic wood gas (20.8%H_2, 13.3%CO, 13.3%CO_2, 6.3%CH_4, 26.8%H_2O, balance N_2 and 0/2032 ppm(vol) $C_{10}H_8$) at 900 °C.

Fig. 9, a magnification of the dotted area marked in Fig. 8 shows the operation curves for synthetic wood gas (20.1% H_2, 13.3% CO, 13.3% CO_2, 6.34% CH_4, 26.8% CH_4 and balance N_2): 1.) without naphthalene, 2.) with 2032 ppm naphthalene and 3.) with 2032 ppm naphthalene considering inhibited methane reforming activity. The idea is to show a scenario regarding the critical distance d_{NiO} to the nickel boundary due to the presence of naphthalene. Starting from curve 1 at $i = i_3$ the H_2-utilization is 70%. In this case complete methane conversion is assumed. Then, the current density is kept constant and naphthalene is added. In this case both CH_4 and naphthalene is said to become reformed completely and thus the point of operation moves onto curve 2 resulting in a lower H_2-utilization rate of 65%. As explained before in Fig. 7 inhibited methane reforming is supposed in the presence of naphthalene. Hence it is assumed that naphthalene replaces methane on the nickel surface. Thus the constraint for the calculation of the ternary plot for operation curve 3 is the assumption that part of the methane passes the anode chamber without taking place in any reaction mechanism. Therefore part of the methane can be seen to be inert and consequently a reduced CH_4 content of 1.64% is taken for the calculation of curve 3 while the rest is substituted by N_2. The reduced CH_4 content is based on the experiment with synthetic wood gas and 2032 ppm naphthalene as described before. By doing this, a reduction of the methane reforming rate from 95% (without naphthalene) down to 35% (with naphthalene) as achieved from the experiment is considered. Keeping a constant current density $i = i_3$ a significant jump of the H_2-utilization up to 91% is predicted since less H_2 is available due to inhibited methane reforming. This situation leads to further risk of nickel oxidation as can be seen by watching the critical distance d_{NiO} between the operation point and the nickel boundary. Presuming that direct oxidation of naphthalene is unlikely higher risk of nickel oxidation in the case of inhibited methane reforming is explained by a faster depletion of H_2 and CO considering a constant current density. Hence the oxygen coming from the cathode could react with the nickel particle.

5. Conclusion

Naphthalene is a critical gas component for the operation of SOFC with wood gas since it inhibits the reforming reactions of other hydrocarbons such as methane. High cell temperatures reduce the inhibition of methane reforming. Therefore it is further necessary to research whether a cell temperature above 900 °C could enable complete reforming of both naphthalene and methane. Furthermore, the current density within the ranges investigated in this work seems not to have any impact on the reforming mechanism. This behaviour suggests the reforming reaction to take place on the nickel surface without interacting with the oxygen coming from the cathode at low H_2-utilization rate.

A further aim is to test synthetic wood gas with lower naphthalene concentrations to find out whether the coverage of the nickel particles by the adsorption of naphthalene reduces. In this case the inhibition of methane reforming could be reduced. If still enough active nickel surface area is available in the presence of naphthalene it is assumed that methane reforming can take place. Another possibility is that merely the period of time until full coverage is reached extends. This test could lead to critical naphthalene limits for the operation of SOFCs with synthetic wood gas. However, wood gas contains a variety of higher hydrocarbons that need to be investigated regarding their mutual impact on the reforming activity. A selection of representative tar species in terms of

concentration and chemical properties has to be picked. Then further experiments with model tars of different molecular structures are intended in order to check whether it is possible to extrapolate from single tar tests to tests with tar mixtures. This is an important step to evaluate wood gas in terms of their application limits in SOFCs.

References

[1] N. Frank, Umsetzung von Kohlenwasserstoffen in SOFCs, Dissertation, Munich, Germany, 2009.
[2] J. P. Ouweltjes, Degradation mechanisms - Influence of hydrocarbons, BioCellus Summer School, Seggau, Austria, 2007.
[3] J. Mermelstein, N. Brandon, M. Millan, Experimental Study Assessment of Mitigation of Carbon Formation on Ni/YSZ and Ni/CGO SOFC Anodes Operating on Biomass Gasification Syngas and Tars, in: European Fuel Cell Forum 2009, Lucerne, Switzerland, 2009.
[4] M. Biber, Messmethoden zur Untersuchung der Kohlenstoffablagerung an nickelhaltigen SOFC-Anoden beim Betrieb mit Methan, Dissertation, Munich, Germany, 2010.
[5] J.-M. Klein, Y. Bultel, S. Georges, M. Pons, Chem. Eng. Sci. 62 (2007) 1636–1649.
[6] N. Laosiripojana, S. Assabumrungrat, J. Power Sources 163 (2007) 943–951.
[7] J.-H. Koh, Y.-S. Yoo, J.-W. Park, H.C. Lim, Solid State Ionics 149 (2002) 157–166.
[8] G.J. Saunders, K. Kendall, J. Power Sources 106 (2002) 258–263.
[9] C.M. Finnerty, R.M. Ormerod, J. Power Sources 86 (2000) 390–394.
[10] C. Fauteux-Lefebvre, N. Abatzoglou, J. Blanchard, F. Gitzhofer, J. Power Sources 195 (2010) 3275–3283.
[11] B.D. Gould, A.R. Tadd, J.W. Schwank, J. Power Sources 164 (2007) 344–350.
[12] H. Tu, U. Stimming, J. Power Sources 127 (2004) 284–293.
[13] A. Weber, B. Sauer, A.C. Müller, D. Herbstritt, E. Ivers-Tiffée, Solid State Ionics 152–153 (2002) 543–550.
[14] D. Shekhawat, D.A. Berry, D.J. Haynes, J.J. Spivey, Fuel 88 (2009) 817–825.
[15] J. Mermelstein, M. Millan, N.P. Brandon, Chem. Eng. Sci. 64 (2009) 492–500.
[16] J. Karl, N. Karellas,N. Frank, H. Spliethoff, Highly efficient conversion of syngas from biomass gasification in Solid Oxide Fuel Cells, in: 14th European Conference and Technology Exhibition on Biomass for Energy, Industry and Climate Protection, Paris, France, 2005.
[17] T. Kienberger, J. Karl, Methanation with an allothermal smart lab-scale gasification system, in: 17th Biomass Conference, Hamburg, Germany, 2009.
[18] J. Karl, Dezentrale Energiesysteme, second ed.; Oldenbourg Verlag München Wien, 2006.
[19] A. Schweiger, Heissgasreinigung, Dissertation, Graz, Austria, 2008.
[20] Ph. Hofmann, A. Schweiger, L. Fryda, K.D. Panopoulos, U. Hohenwarter, J.D. Bentzen, J.P. Ouweltjes, J. Ahrenfeldt, U. Henriksen, E. Kakaras, J. Power Sources 173 (2007) 357–366.
[21] Ph. Hofmann, K.D. Panopoulos, P.V. Aravind, M. Siedlecki, A. Schweiger, J. Karl, J.P. Ouweltjes, E. Kakaras, J. Hydrogen Energy 34 (2009) 9203–9212.
[22] Ph. Hofmann, A. Schweiger, L. Fryda, K. D. Panopoulos, U. Hohenwarter, J. P. Ouweltjes, J. Karl, E. Kakaras, Results from planar SOFCs operated on hot cleaned gas derived from two experimental gasification facilities, in: 15th European Biomass Conference & Exhibition, Berlin, Germany, 2007.
[23] T. Kienberger, J. Karl, Tests on methanation with tar and sulphur loaded syngas. In: 1st International Conference on Polygeneration Strategies, Vienna, Austria, 2009.
[24] M. Hauth, N. Frank, J. Karl, Influence of Tars on the Maxium Hydrogen Utilization in SOFCs with Biogeneous Gases, In: European Fuel Cell Forum 2009, Lucerne, Switzerland, 2009.
[25] A. Jess, Chem. Eng. Process. 35 (1996) 487–494.
[26] A. Jess, Fuel 75 (12) (1996) 1441–1448.
[27] S. C. Singhal, K. Kendall, High Temperature Solid Oxide Fuel Cells - Fundamentals, Design and Applications, Elsevier Ltd. 2003, ISBN 1856173879.
[28] J. Xu, G. Froment, AIChE J. 35 (1) (1989) 88–96.
[29] H. Depner, A. Jess, Fuel 78 (1999) 1369–1377.